International Journal of Mass Spectrometry 311 (2012) 17–23

Contents lists available at SciVerse ScienceDirect

International Journal of Mass Spectrometry

journal homepage: www.elsevier.com/locate/ijms

Microhydrated cobalt-nitrate cations $[Co(NO_3)(H_2O)_n]^+$ ($n = 2, 3$) studied by infrared spectroscopy in the gas phase

Christopher J. Shaffer, Detlef Schröder*

Institute of Organic Chemistry and Biochemistry, Flemingovo nám. 2, 16610 Prague, Czech Republic

ARTICLE INFO

Article history:
Received 29 September 2011
Received in revised form
18 November 2011
Accepted 18 November 2011
Available online 16 December 2011

Keywords:
Cobalt nitrate
Density functional theory
Electrospray ionization
Infrared spectroscopy
Kinetic modeling
Microhydration

ABSTRACT

The microhydrated cations $[Co(NO_3)(H_2O)_n]^+$ ($n = 2, 3$) generated via electrospray ionization of aqueous cobalt(II) nitrate are studied by means of infrared-multiphoton dissociation (IRMPD) spectroscopy in an ion-trap mass spectrometer (IT-MS) at the free electron laser CLIO. While $[Co(NO_3)(H_2O)_3]^+$ shows a simple photo-induced fragmentation upon IRMPD, the situation is more complex for $[Co(NO_3)(H_2O)_2]^+$ because during storage in the IT-MS the ion associates with background water to afford $[Co(NO_3)(H_2O)_3]^+$, and both species adsorb IR photons in the same range. By means of kinetic modeling, it is demonstrated that also in such a more complicated situation useful insights can be achieved. For all $[Co(NO_3)(H_2O)_n]^+$ cations studied ($n = 0$–3) in parallel theoretical studies, a bidentate coordination of the nitrato ligand is preferred, and this conclusion finds support by a comparison of the computed and experimental IR spectra. In addition, the binuclear cluster $[Co_2(NO_3)_3(H_2O)_3]^+$ is probed by means of IRMPD.

1. Introduction

The microsolvation of gaseous ions, microhydration in particular [1], receives continuous interest because it can help to provide a first-principle understanding of ion solvation with the ultimate aim to link gas-phase properties with observations in the condensed phase [2]. In this context, metal nitrates have attracted significant attention [3–5] because nitrate is a frequent counter ion in metal processing [6] and also can serve as an oxidant in either catalytic processes themselves or in the preparation of metal-oxide catalysts [7], including nanomaterials [8,9]. The oxidative power of the nitrate counterion has also been exploited for the generation of reactive metal-oxide species in the gas phase via electrospray ionization (ESI) of aqueous solutions of the corresponding nitrates [10,11], e.g., MgO^+ [12], FeO^+ [13], (1,10-phenanthroline)CuO^+ [14], and Ag_2O^+ [15]. Similarly, a series of redox reactions involved in the dissociation of microhydrated $[Co_m(NO_3)_{2m-1}(H_2O)_n]^+$ cations in the gas phase have been described recently [16]. Here, we report an investigation of some of these cobalt-nitrate cations by means of infrared-multiphoton dissociation (IRMPD [17–19]) spectroscopy with the aim of providing information about the coordination geometry of the nitrato ligand in contact ion pairs with cobalt because a nitrate counterion can bind to a metal cation either with one or two of its oxygen atoms, i.e., mono- versus bidentate coordination [20–22]. The coordination mode of such an ambident ligand can in turn crucially be influenced by the presence of additional ligand or solvent molecules which may alter the coordination mode of the ligand [22,23] and also the electronic state of the metal ion [24–26].

2. Experimental and theoretical details

Initial mass spectrometric measurements were performed with a Finnigan LCQ Classic ion-trap mass spectrometer (IT-MS [27]) by ESI of dilute aqueous solutions of cobalt(II) nitrate. In brief, the LCQ bears a conventional ESI source consisting of the spray unit (typical flow rates between 5 and 30 μl/min, typical spray voltage 5 kV) with nitrogen as a sheath gas, followed by a heated transfer capillary (kept at 200 °C), a first set of lenses which determines the soft- or hardness of ionization by variation of the degree of collisional activation in the medium pressure regime [28,29], two transfer octopoles, and a Paul ion-trap with ca. 10^{-3} mbar helium for ion storage and manipulation, including a variety of MS^n experiments [30]. For detection, the ions are ejected from the trap to an electron multiplier. Comparison of the expected isotopic pattern of various ions with the experimentally measured peak heights confirmed all ion assignments made below. Low-energy CID was performed by application of an excitation AC voltage to the end caps of the trap to induce collisions of the isolated ions with the helium buffer gas for a period of 20 ms [31,32].

* Corresponding author. Tel.: +420 220 183 463; fax: +420 220 183 462.
E-mail address: Detlef.Schroeder@uochb.cas.cz (D. Schröder).

1387-3806/$ – see front matter © 2011 Elsevier B.V. All rights reserved.
doi:10.1016/j.ijms.2011.11.012

In addition, gas-phase infrared spectra of the mass-selected cations $[Co(NO_3)(H_2O)_2]^+$ and $[Co(NO_3)(H_2O)_3]^+$, and $[Co_2(NO_3)_3(H_2O)_3]^+$ were recorded with a Bruker Esquire 3000 IT-MS [33–35] mounted to a beamline of the free electron laser at CLIO (Center Laser Infrarouge Orsay, France). The ions of interest were generated by ESI from aqueous solution as described above and transferred into the ion trap; the major differences between the ion sources of the LCQ and the Esquire IT-MS is that in the former the spray is on axis with the transfer capillary made from stainless steel, whereas the spray and the quartz transfer capillary form a 90° arrangement in the latter. The overall mass spectra were similar in both instruments, while the abundance ratios somewhat differed. After mass-selection, infrared multi-photon dissociation (IRMPD) was induced by admittance of a single pulse of IR-laser light from CLIO to the ion trap, resulting in a total cycling time of about half a second. For each wavelength (step size ca. 4 cm^{-1}), 8 scans were averaged to one mass spectrum which was stored, the procedure was repeated 3 times before the wavelength was changed and the data again averaged, such that each data point in the IRMPD spectra consists of 32 scans. Further, all IRMPD spectra were independently recorded at least two times and the spectra shown are the averaged scans. In the 45 MeV range in which CLIO was operated in these experiments, the IR light covers a spectral range from about 1000 to 2000 cm^{-1}. In this spectral region, half widths of <20 cm^{-1} have been achieved in some cases at CLIO [36,37], but often the line widths are significantly broader due to the presence of several conformations. Note that in this kind of action spectra, the assumption that the amount of ion fragmentation is proportional to the IR absorbance is not always justified due to the multiphotonic nature of IRMPD. Thus, the major analytical weight is put on the peak positions, rather than the peak heights in the IRMPD spectra [38–40].

Ab initio calculations were performed with density functional theory using the B3LYP hybrid functional [41–44]. Atoms were described by 6-311+G(2d,p) basis sets as implemented in the Gaussian 09 suite [45]. For all optimized structures, frequency analysis at the same level of theory was performed in order to assign them as genuine minima or transition structures on the potential-energy surface as well as to calculate zero-point vibrational energies. The relative energies (E_{rel}) of the structures given below thus refer to energies at 0 K in the gaseous state; solvation, aggregation, etc. are deliberately not included, in order to match the present experimental conditions. For comparison of the calculated IR spectra with the IRMPD data in Fig. 1, we apply a common scaling factor [46] of 0.98 based on comparison of the computed and experimental frequencies of free HNO_3 [47]. In order to probe the sensitivity of the computed IR spectra with regard to the theoretical method, additional calculations were performed with the TPSSH density functional which is assumed to perform particularly well for metal compounds [48], but no particular observations in comparison with experiments were made nor any trends became obvious.

3. Results and discussion

Prior to the IRMPD studies, the microhydrated cobalt(II) nitrate cations were screened and characterized using a Finnigan LCQ Classic ion trap mass spectrometer. Under mild conditions in the ion source [28,29,49,50], electrospray ionization (ESI) of an aqueous solution of $Co(NO_3)_2$ yields the microsolvated $[Co(NO_3)(H_2O)_n]^+$ monocations with n up to 4 as the leading cationic species, along with some polynuclear clusters of the general formula $[Co_m(NO_3)_{2m-1}(H_2O)_n]^+$ [16,51,52]. Upon collisional activation, these cluster ions either loose water ligands (reaction (1)) or undergo cluster degradation to the corresponding lower members of the series concomitant with release of cobalt(II) nitrate as a neutral fragment (reaction (2)) with the corresponding mononuclear cobalt complexes as the quasi-terminal fragments of the series. To a limited extent, also N—O bond cleavages of the nitrato ligands are observed, which have been discussed elsewhere [16,53] and are not pursued here any further.

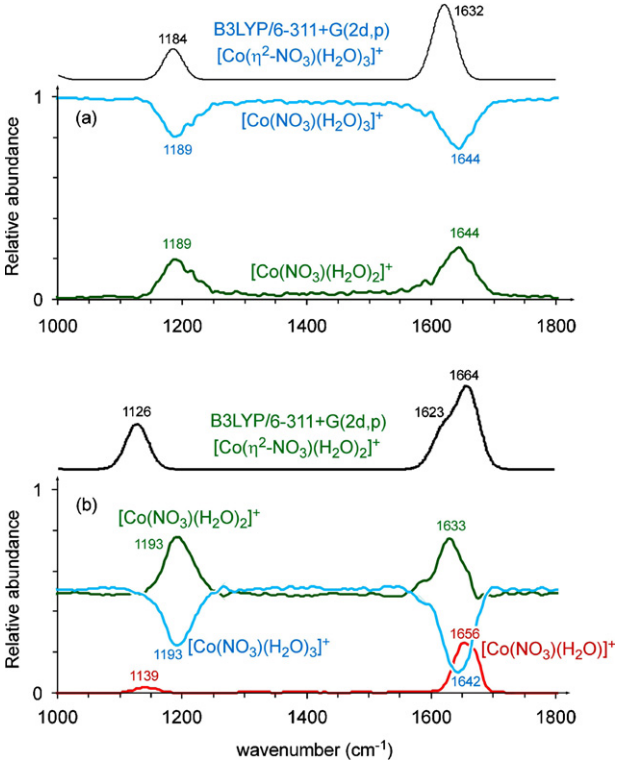

Fig. 1. Precursor, fragment, and adduct ion yields in the IRMPD mass spectra of (a) mass-selected $[Co(NO_3)(H_2O)_3]^+$ (m/z 175, blue) and (b) $[Co(NO_3)(H_2O)_2]^+$ (m/z 157, green) in the range from 1000 to 1800 cm^{-1}. Note that the trace of $[Co(NO_3)(H_2O)]^+$ in (b) includes all subsequent fragments such as $Co(OH)_2^+$ [16,53]. The panels on top of the experimental IRMPD spectra show the respective computed IR transitions of $[Co(\eta^2\text{-}NO_3)(H_2O)_n]^+$ ($S = 3/2$) in this spectral region (frequencies scaled by 0.98). (For interpretation of the references to color in this figure legend and in text, the reader is referred to the web version of this article.)

$$[Co_m(NO_3)_{2m-1}(H_2O)_n]^+ \rightarrow [Co_m(NO_3)_{2m-1}(H_2O)_{n-1}]^+ + H_2O \quad (1)$$

$$[Co_m(NO_3)_{2m-1}(H_2O)_n]^+ \rightarrow [Co_{m-1}(NO_3)_{2m-3}(H_2O)_n]^+ + Co(NO_3)_2 \quad (2)$$

Similar to collisional activation, ion dissociation can also be brought about by infrared photons provided that a sufficiently intense light source is used because typical hydration energies of gaseous ions are about 100 kJ mol^{-1}, which is much more than the energy of an IR photon in the fingerprint region (about 10–20 kJ mol^{-1}). However, occurrence of energy transfer from the laser beam to the mass-selected ions in the trap requires the existence of IR-active modes in the wavelength regime sampled in the IRMPD experiment. Resonant absorption leads to ion heating followed by dissociation. Monitoring the fragment ion products as a function of IR photon wavelength thus enables us to record the infrared spectra for mass-selected ions in the gas phase.

Fig. 1 shows the IRMPD data obtained for $[Co(NO_3)(H_2O)_2]^+$ and $[Co(NO_3)(H_2O)_3]^+$, of which we discuss the latter species first, because for the bishydrated ion, the experimental situation is more complex. In IRMPD, the infrared spectrum of a mass-selected ion is monitored via its fragmentation ("action spectroscopy"). Hence, the parent ion is the only species in the spectrum if no IR adsorption occurs, whereas the fragment ions appear whenever

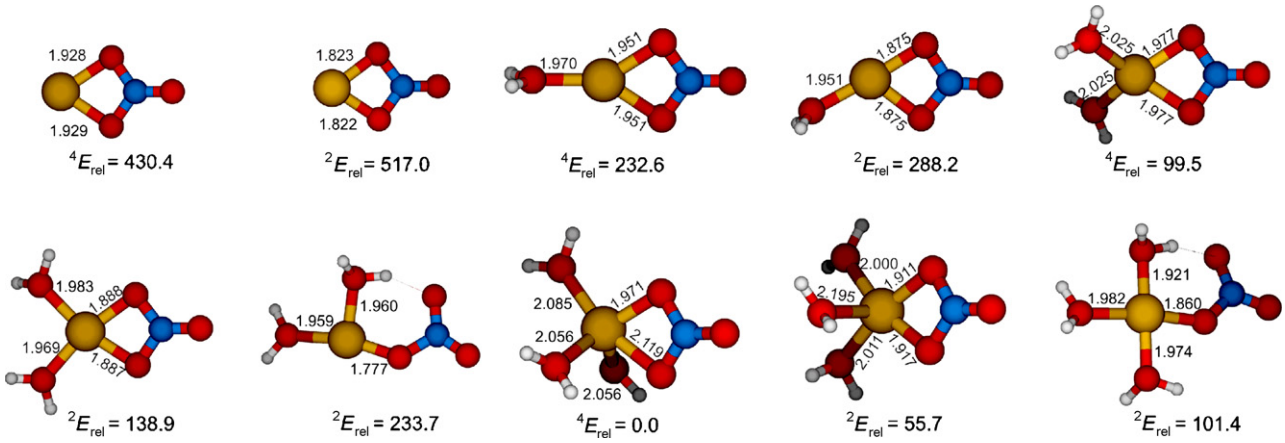

Fig. 2. Computed structures and relative energies of $[Co(NO_3)(H_2O)_n]^+$ ions for n = 0–3 with selected bond lengths given in Angstrom. The relative energies (E_{rel} in kJ mol^{-1}) refer to the most stable structure of $[Co(NO_3)(H_2O)_3]^+$ with a η^2-coordinated nitrato ligand in the quartet (S = 3/2) spin state (additional free water molecules for the fragment ions are omitted).

an IR active mode is excited. Accordingly, the IRMPD spectrum of $[Co(NO_3)(H_2O)_3]^+$ (Fig. 1a) shows two bands that coincidentally decrease the parent ion yield and increase fragment ion yields at 1189 and 1644 cm^{-1}, respectively; for comparison, the computed spectrum of the most stable structure (see below) is shown on top of the experimental data. We further note that during the same beam-time period at CLIO, much more narrow bands were obtained for other ions [39,54]. The relatively large width of the spectral features in Fig. 1 is hence not a result of experimental conditions, but an inherent property of the systems under study, such as the presence of different conformers and the flexibility of the ligand environment under the storage conditions in an ion trap. A further structural assignment is made in the context of theoretical results discussed below.

$$[Co(NO_3)(H_2O)_2]^+ + H_2O \rightarrow [Co(NO_3)(H_2O)_3]^+ \quad (3)$$

$$[Co(NO_3)(H_2O)_2]^+ + h\nu \rightarrow [Co(NO_3)(H_2O)]^+ + H_2O \quad (4)$$

$$[Co(NO_3)(H_2O)_3]^+ + h\nu \rightarrow [Co(NO_3)(H_2O)_2]^+ + H_2O \quad (5)$$

In the case of $[Co(NO_3)(H_2O)_2]^+$, the situation is more complex because within the time required for a complete cycle of the IR laser experiment at CLIO this particular ion associates with water present in the background of the ion-trap mass spectrometer [24,37,55] to form the trishydrated ion $[Co(NO_3)(H_2O)_3]^+$ (reaction (3)). Hence, in the absence of IR adsorption, a ca. 1:1 ratio of $[Co(NO_3)(H_2O)_2]^+$ and $[Co(NO_3)(H_2O)_3]^+$ is observed (Fig. 1b). Only if IR active modes are excited, photodissociation to $[Co(NO_3)(H_2O)]^+$ (reaction (4)) and subsequent fragmentations [16] are observed. In addition, however, the parent ion $[Co(NO_3)(H_2O)_2]^+$ shows a dramatic increase in relative abundance, which can be attributed to two simultaneous effects: (i) the IR-induced photofragmentation of $[Co(NO_3)(H_2O)_3]^+$ (reaction (5)) and (ii) hindrance of the association of $[Co(NO_3)(H_2O)_2]^+$ with water (reaction (3)) upon ion excitation and hence increasing internal energy. Accordingly, the ion traces in Fig. 1b result from a superposition of the IR spectra of two different ionic species, namely, the $[Co(NO_3)(H_2O)_2]^+$ precursor and its water adduct $[Co(NO_3)(H_2O)_3]^+$. The result looks similar to a difference spectrum, but it is in fact just the consequence of the opposing effects caused by the occurrence of reactions (3)–(5), where reactions (3) and (4) serve as sinks for the $[Co(NO_3)(H_2O)_2]^+$ precursor ion, while reaction (5) acts as a feed. Within the experimental uncertainties, the peak positions in the traces for $[Co(NO_3)(H_2O)_2]^+$ (green) and $[Co(NO_3)(H_2O)_3]^+$ (blue) agree in Fig. 1a and b, whereas the low-frequency mode in the $[Co(NO_3)(H_2O)]^+$ fragment channel is shifted to 1139 cm^{-1} (red trace in Fig. 1b). A conceptual question arising in this context is whether or not IRMPD data such as in Fig. 1b can be deconvoluted to distinguish the spectra of the separate components, and we return to this aspect further below.

Density functional theory (B3LYP/6-311+G(2d,p)) predicts a bidentate coordination of the nitrato group in all $[Co(NO_3)(H_2O)_n]^+$ complexes with n = 0–4 (Fig. 2). Further, in the η^2-structures the quartet states are clearly favored over the corresponding doublets with doublet/quartet gaps no smaller than 38 kJ mol^{-1}. As far as monodentate binding of the nitrato ligand is concerned, the quartet states of the η^1-complexes unavoidably converted into the corresponding η^2-structures during geometry optimization. Similarly, for n = 0 and 1, the structures with monodentate coordination in the S = 1/2 system could not be localized as minima, whereas for n = 2 the η^1-structure lies 95 kJ mol^{-1} higher in energy than the η^2-complex, and this difference decreases to 46 kJ mol^{-1} for n = 3. For n = 4, the η^2-complex is only favored by 24 kJ mol^{-1}, but the quartet state of the η^2-complex is still favored by 62 kJ mol^{-1}. Thus, the monodentate coordination is disfavored at low coordination numbers, even though some stabilization by hydrogen bonding between one of the water ligands and one of the oxygen atoms of the nitrato ligand occurs in the η^1-structures with n = 2 and 3. The bond lengths behave as expected in that all metal—ligand bonds are slightly elongated upon increase of the coordination number. Notable is the Co—O distance of the third water ligand in doublet $[Co(\eta^2\text{-}NO_3)(H_2O)_3]^+$ which amounts to almost 2.2 Å compared to values of about 2.0 Å in all other complexes, indicating that the quasi square-planar coordination in doublet $[Co(\eta^2\text{-}NO_3)(H_2O)_2]^+$ is partially maintained also in doublet $[Co(\eta^2\text{-}NO_3)(H_2O)_3]^+$. In contrast to the doublet system, when n = 3 for the quartet state, the Co—O hydrate bond distances are more uniformly centered around 2.05 Å. Another notable observation with regard to the computed structures is that the η^2-nitrato ligand is bound quasi-symmetrically with almost identical Co—O bond lengths for n = 0–2, whereas in quartet $[Co(\eta^2\text{-}NO_3)(H_2O)_3]^+$ one of the Co—O bonds is significantly elongated (1.97 Å vs. 2.12 Å). Consistent with previous studies [56], a square-planar structure is not preferred in the quartet system and thus at n = 2, a tetrahedral structure is encouraged.

With regard to the quartet ground states (S = 3/2), the sequential hydration energies amount to 198 kJ mol^{-1} for water association to the bare $Co(NO_3)^+$ cation, 133 kJ mol^{-1} for $[Co(NO_3)(H_2O)]^+$, followed by an even further decrease to 100 kJ mol^{-1} for binding of a third water ligand to $[Co(NO_3)(H_2O)_2]^+$. A fourth water coordination to $[Co(NO_3)(H_2O)_3]^+$ brings only 35 kJ mol^{-1}. Compared to other metal-nitrate cations (Fig. 3), the relative decrease of the

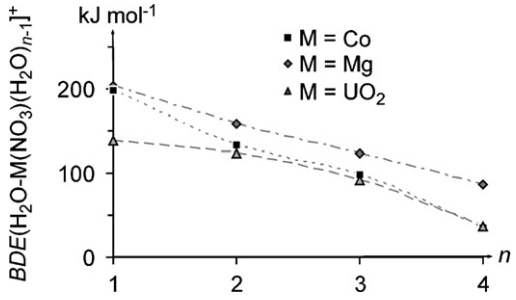

Fig. 3. Sequential water binding energies of the cations $Mg(NO_3)^+$ [57], $Co(NO_3)^+$, and $UO_2(NO_3)^+$ [58] as a function of the number of water ligands n.

binding energy drops significantly per addition of water, which can be understood in terms of changes in polarization as addressed below.

For comparison with the experimental IRMPD spectra, the computed frequencies of the $[Co(NO_3)(H_2O)_n]^+$ cations are listed in Table 1. In general, the spectral signatures of the mono- and bidentate coordination geometries are similar in the region from 1600 to 1700 cm^{-1}, where a substantial overlap occurs with HO—H bending modes (also see Appendix A). In contrast, significant differences appear in the range between 1100 and 1300 cm^{-1}. Specifically, the ONO asymmetric stretch of the metal coordinated O-atoms is predicted to red-shift up to 120 cm^{-1} in comparing monodentate and bidentate complexes. For both ions studied experimentally (Fig. 1), the spectra computed for the bidentate complexes are in significantly better agreement than those of the structures with monodentate nitrato ligands. This assignment is further supported by the preferential energetics of the bidentate structures compared to the monodentate forms. Furthermore, the experimentally observed red-shift of the CoO—NO antisymmetric stretching mode from 1193 cm^{-1} in $[Co(NO_3)(H_2O)_3]^+$ to 1139 cm^{-1} in $[Co(NO_3)(H_2O)_2]^+$ ($\Delta\nu = 54\ cm^{-1}$) is consistent with the computed red-shift of $\Delta\nu = 58\ cm^{-1}$ for the bidentate structures, whereas this mode is predicted to exhibit a blue shift for the computed monodentate structures (Table 1).

Elaborating on the N—O modes further, the experimental peaks at 1139 and 1656 cm^{-1} give a difference of 517 cm^{-1} for the two observed antisymmetric nitrate (υ_3) modes [21]. The higher frequency component is assigned to stretching of the terminal, non-coordinating N=O moiety, whereas the lower frequency is attributed to the antisymmetric stretching of the coordinated oxygen atoms. The magnitude of this splitting ($\Delta\upsilon_3$) has been correlated with the polarizing power of the coordinating cation, such that a sizeable difference is noticed in perturbations as small as the difference between alkali and alkaline earth metals [59]. Typically, this results in $\Delta\upsilon_3$ values of about 270 cm^{-1}, but for matrix isolated $Cu(NO_3)_2$ the value $\Delta\upsilon_3$ has been found to be as high as 410 cm^{-1}. A further increase in the effective charge state in the gaseous ions may help to bring this value to 517 cm^{-1} in $[Co(NO_3)(H_2O)_2]^+$, while in $[Co(NO_3)(H_2O)_3]^+$ an increase in water coordination weakens the NO_3 binding energy and thus lowers $\Delta\upsilon_3$ to 455 cm^{-1}.

Finally, the enlarged width of the IRMPD peaks may be understood in terms of a dynamic equilibrium of the ion population with minor contributions from structures with η^1-nitrato ligands which bear the CoO—NO_2 bending mode above 1200 cm^{-1}. In addition, the IRMPD spectrum of the dinuclear cluster $[Co_2(NO_3)_3(H_2O)_3]^+$ was recorded (Fig. 4), which shows two broad bands around 1256 and 1625 cm^{-1}, respectively, and a weaker shoulder at 1030 cm^{-1}. While we did not perform calculations on this dinuclear species, comparison of the general trends might suggest contributions from monodentate coordination because the CoO—NO stretching mode appears above 1200 cm^{-1}, as found for the monodentate structures

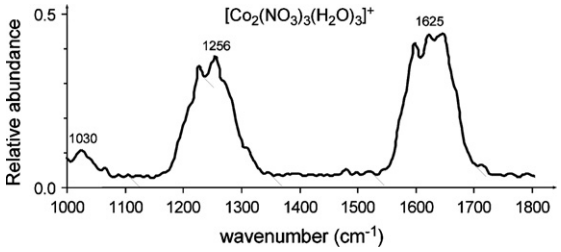

Fig. 4. IRMPD spectrum of mass-selected $[Co_2(NO_3)_3(H_2O)_3]^+$ (m/z 358) in the range from 1000 to 1800 cm^{-1}.

of the mononuclear complexes (Table 1). Similarly, the shoulder at 1030 cm^{-1} lies in the position of the additional HO—H bending mode at 1076 cm^{-1} (scaled: 1054 cm^{-1}) found for the mononuclear complex $[Co(NO_3)(H_2O)_3]^+$. Note, however, that in the binuclear clusters the modified modes of the bridging nitrato ligands are also expected in this frequency range [21]. Moreover, the significant broadening of the bands in the experimental spectrum indicates the presence of a mixture of conformers [54,60,61].

Finally, we asked ourselves, if the assumption that the trace for the appearance of $[Co(NO_3)(H_2O)]^+$ fragments corresponds to the IR spectrum of $[Co(NO_3)(H_2O)_2]^+$ is justified for a convoluted IRMPD spectrum like that shown in Fig. 1b. To this end, we made a kinetic modeling [62–65] adapted to the time sequence of the IRMPD experiment. As illustrated at the top of Fig. 5, the IRMPD experiment consists of several steps: (i) filling of the trap with ions generated in the ESI source, (ii) mass-selection of the ion of interest, (iii) a time delay prior to the first laser pulse entering the trap, (iv) arrival of the laser pulse followed by prompt photodissociation, and (v) a final trapping period followed by ion detection. In the kinetic modeling, we mimic this time sequence by starting with 100% of the precursor ion ($[Co(NO_3)(H_2O)_2]^+$) after mass-selection, then allowing it to associate with background water in the delay before the laser pulse, followed by photodissociation within the IR laser pulse and again association with water in the final delay prior to detection. The corresponding kinetic scheme is shown in the central box in Fig. 5; for details see Appendix B.

Using the frequencies given in Fig. 1b and the amount of hydration in the absence of IR absorption as input parameters, this simple kinetic model is able to reasonably well reproduce the experimental data points (lower panel of Fig. 5). The acceptable fit thereby

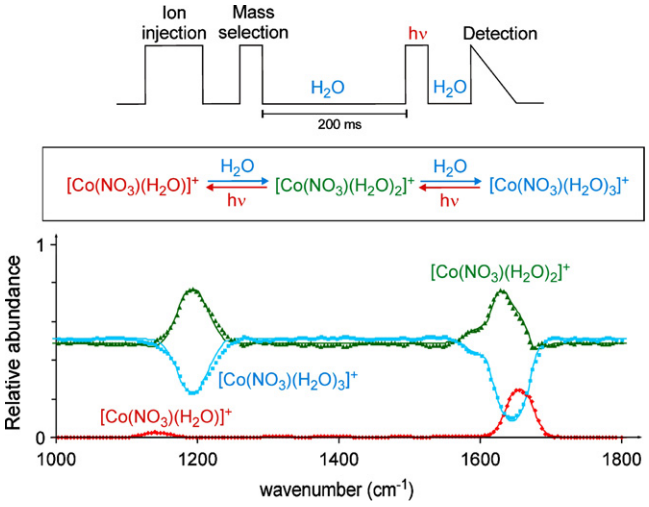

Fig. 5. Scheme of the IRMPD sequence, the kinetic model for the water association of $[Co(NO_3)(H_2O)_2]^+$ in competition with photon-induced dissociation, and the result of a kinetic modeling (lines) of the experimental data in Fig. 1b (symbols).

Table 1
Computed IR frequencies (scaling factor 0.98) and intensities (in brackets, in km mol^{-1}) of $[Co(NO_3)(H_2O)_n]^+$ cations (n = 0–3) in the range of 800–2000 cm^{-1}.

	Monodentate (η^1)[a]		Bidentate (η^2)[b]	
$[Co(NO_3)]^+$			ON—O_2 stretch	926 (67)
			CoO—NO stretch	1070 (195)
			O—NO_2 stretch	1711 (401)
$[Co(NO_3)(H_2O)]^+$			ON—O_2 stretch	952 (65)
			CoO—NO stretch	1118 (233)
			HO—H bending	1640 (100)
			O—NO_2 stretch	1688 (485)
$[Co(NO_3)(H_2O)_2]^+$	ON—O_2 stretch	858 (260)	ON—O_2 stretch	952 (69)
	HO—H bending	890 (255)		
	CoO—NO_2 stretch	1245 (222)	CoO—NO stretch	1126 (262)
	HO—H bending	1596 (178)	HO—H bending	1623 (178)
	HO—H bending	1628 (124)	HO—H bending	1627 (49)
	ON—O_2 stretch	1659 (299)	O—NO_2 stretch	1664 (456)
$[Co(NO_3)(H_2O)_3]^+$	ON—O_2 stretch	948 (254)	ON—O_2 stretch	981 (77)
	HO—H bending	1054 (315)[c]		
	CoO—NO_2 stretch	1222 (272)	CoO—NO stretch	1184 (303)
	HO—H bending	1584 (339)	HO—H bending	1611 (189)
	HO—H bending	1614 (149)	HO—H bending	1613 (99)
	HO—H bending	1619 (45)	HO—H bending	1622 (169)
	ON—O_2 stretch	1639 (192)	O—NO_2 stretch	1632 (404)

[a] Doublet states (S = 1/2); for the quartet, the monodentate structures had no minima.
[b] Quartet states (S = 3/2); the doublet states are omitted because these are significantly higher in energy (see Fig. 2).
[c] This bending mode is perturbed due to its involvement in a hydrogen bonding interaction with the monodentate nitrate.

demonstrates that even for a complex situation like in the case of $[Co(NO_3)(H_2O)_2]^+$ useful infrared patterns can be extracted from IRMPD fragment appearance data.

4. Conclusions

The infrared spectra of microhydrated cobalt(II) nitrate ions $[Co(NO_3)(H_2O)_n]^+$ (n = 2, 3) in combination with parallel theoretical calculations reveal a preference for a bidentate coordination of the nitrato ligands to cobalt at low degrees of water coordination. However, the energetic disadvantage of the monodentate structures decreases with an increase in hydration, suggesting that this bonding motif might be populated in solution [4,51]. Further, the IRMPD spectrum of mass-selected $[Co(NO_3)(H_2O)_2]^+$ shows a complex pattern, caused by competition of association with water present in the background and loss of water via photodissociation when infrared-active bands are excited. It is demonstrated that this situation can be understood qualitatively by a combination of three elementary reactions and quantitatively reproduced by means of kinetic modeling, thereby allowing the extraction of the infrared patterns of the separate components from convoluted IRMPD patterns.

Acknowledgments

This work was supported by the Academy of Sciences of the Czech Republic (Z40550506) and the European Research Council (AdG HORIZOMS). The mission to CLIO was supported within the ELISA program of the European Commission. We thank Mgr. Lucie Jašiková and the team of CLIO for their kind assistance during the measurements.

Appendix A. Water bending modes of microhydrated metal ions

One reviewer doubted that the water bending modes in the region around 1600 cm^{-1} can be seen with IRMPD and therefore asked us to include a species such as $[(H_2O)_nCoCl]^+$ in future IRMPD experiments. While we have reported such modes in several previous studies [57,66–69], these might indeed be questioned because the additional anionic ligands involved in these particular studies also have bands in this spectral region. However, in a different context we have previously recorded an IRMPD spectrum of $[(H_2O)_2FeI]^+$ which is shown in Fig. A1. Because in this case the only IR active modes are those of the water ligands, the band observed at about 1646 cm^{-1} demonstrates beyond any doubts that the bending modes of the water ligands can be observed with IRMPD. Further, the experimental spectrum agrees well with the computed spectrum of $[Fe(H_2O)_2I]^+$ (B3LYP/3-21G), which shows two major bands are 1629 and 1651 cm^{-1} (scaling factor 0.97) for the in-plane and out-of-plane water bending modes.

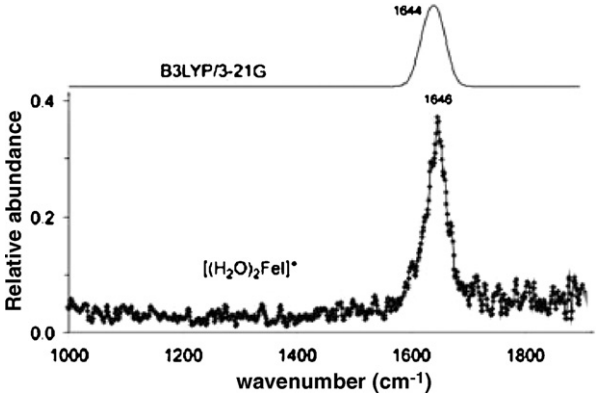

Fig. A1. IRMPD spectrum of mass-selected $[(H_2O)_2FeI]^+$ (m/z 219) in the range from 1000 to 1900 cm^{-1}. The noise is elevated compared to Fig. 1 because $[(H_2O)_2FeI]^+$ undergoes some background dissociation upon trapping and because only a single spectrum with few accumulations was taken.

Appendix B. Kinetic modeling of the IRMPD experiment with competing association

In the kinetic modeling of the IRMPD experiment with $[Co(NO_3)(H_2O)_2]^+$, for the sake of simplicity we assume an evolution of the ion population in three, fully independent steps.

The first phase is the pre-trap after the mass-selection of $[Co(NO_3)(H_2O)_2]^+$ during which association with background water leads to the formation of $[Co(NO_3)(H_2O)_3]^+$, while all dissociations are neglected in the model. During the arrival of the IR laser pulse, wavelength-dependent photodissociation via water losses is allowed to take place, while associations are neglected. After the

laser pulse, a final trapping phase prior to detection again allows the ion population to add water molecules from the background, while dissociations are neglected. Hence, the abundances of the precursor ion $I([Co(NO_3)(H_2O)_2]^+)$, of the desolvated ion $I([Co(NO_3)(H_2O)]^+)$, and of the hydration product $I([Co(NO_3)(H_2O)_3]^+)$ are given by the following time sequence, in which we denote them only by the number of water ligands, i.e., $I(n=1)$, $I(n=2)$, and $I(n=3)$, respectively, and likewise the model functions f_{IR} and the phenomenological terms ε_{IR} are abbreviated as $f_{IR}(n=2)$ and $f_{IR}(n=3)$ as well as $\varepsilon_{IR}(n=2)$ and $\varepsilon_{IR}(n=3)$, respectively.

Mass selection ($t=0$)

$$I(n=1)_{t=0} = 0$$

$$I(n=2)_{t=0} = 1$$

$$I(n=3)_{t=0} = 0$$

Pretrap ($t_{pre} = 200\,ms$)

$$I(n=1)_{pre} = 0$$

$$I(n=2)_{pre} = I(n=2)_{t=0} \cdot \exp(-k_a \cdot t_{pre})$$

$$I(n=3)_{pre} = I(n=2)_{t=0} \cdot (1 - \exp(-k_a \cdot t_{pre}))$$

IRMPD (t_{IR} < ms, association thus neglected)

$$I(n=1)_{IR} = I(n=2)_{pre} \cdot (1 - \exp(-f_{IR}(n=2) \cdot \varepsilon_{IR}(n=2)))$$

Note: Because all subsequent smaller fragments are summed-up in the trace of $[Co(NO_3)(H_2O)]^+$, photon-induced dissociation of this ion is neglected. The term ε_{IR} represents the relative abundance of photofragmentation.

$$I(n=2)_{IR} = I(n=2)_{pre} \cdot \exp(-f_{IR}(n=2) \cdot \varepsilon_{IR}(n=2)) + I(n=3)_{pre} \cdot (1 - \exp(-f_{IR}(n=3) \cdot \varepsilon_{IR}(n=3)))$$

Note: For the sake of simplicity, photon-induced dissociation of $[Co(NO_3)(H_2O)_3]^+$ is assumed to exclusively yield $[Co(NO_3)(H_2O)_2]^+$.

$$I(n=3)_{IR} = I(n=3)_{pre} \cdot \exp(-f_{IR}(n=3) \cdot \varepsilon_{IR}(n=3))$$

Posttrap ($t_{post} = 20\,ms$)

$$I(n=1)_{final} = I(n=1)_{IR} \cdot \exp(-k_{a'} \cdot t_{post})$$

$$I(n=2)_{final} = I(n=2)_{IR} \cdot \exp(-k_a \cdot t_{post}) + I(n=1)_{IR}\,(1 - \exp(-k_{a'} \cdot t_{post}))$$

$$I(n=3)_{final} = I(n=3)_{IR} + I(n=2)_{IR} \cdot (1 - \exp(-k_a \cdot t_{post}))$$

The term $f_{IR}(i)$ is a simplistic representation of the IR spectrum in the wavelength regime covered given as a sum of the minimal amount of Gaussian functions required to model the experimental patterns of $[Co(NO_3)(H_2O)_2]^+$ and $[Co(NO_3)(H_2O)_3]^+$, respectively, within the signal-to-noise ratio. The fit of the former ion requires two Gaussians centered at $1142\,cm^{-1}$ ($f_{IR} = 0.06$) and $1656\,cm^{-1}$ ($f_{IR} = 1$), respectively, while the fit for the latter is requires three Gaussians centered at $1193\,cm^{-1}$ ($f_{IR} = 0.42$), $1595\,cm^{-1}$ ($f_{IR} = 0.07$), and $1644\,cm^{-1}$ ($f_{IR} = 1$), respectively. For the relative photodissociation efficiencies, the best fit requires $\varepsilon_{IR}(n=2) = 0.51$ and $\varepsilon_{IR}(n=3) = 0.9$, respectively. The fit of the ratio of the ions with $n=2$ and $n=3$ in the absence of IR-absorption requires $k_a = 3.25\,s^{-1}$ and the best value for $k_{a'}$ is $21\,s^{-1}$.

References

[1] M.K. Beyer, Mass Spectrom. Rev. 26 (2007) 517.
[2] P. Jungwirth, Faraday Disc. 141 (2009) 9.
[3] A. Wahab, S. Mahiuddin, G. Hefter, W. Kunz, B. Minofar, P. Jungwirth, J. Phys. Chem. B 109 (2005) 24108.
[4] B. Minofar, R. Vacha, A. Wahab, S. Mahiuddin, W. Kunz, P. Jungwirth, J. Phys. Chem. B 110 (2006) 15939.
[5] T. Megyes, S. Balint, E. Peter, T. Grosz, I. Bako, H. Krienke, M.C. Bellissent-Funel, J. Phys. Chem. B 113 (2009) 4054.
[6] E.P. Horwitz, D. Kalina, H. Diamond, G. Vandergrift, W. Schulz, Solvent Extr. Ion Exc. 3 (1985) 75.
[7] J.G. Jackson, A. Novichikhin, R.W. Fonseca, J.A. Holcombe, Spectrochim. Acta B 50 (1995) 1423.
[8] J.R.A. Sietsma, J.D. Meeldijk, J.P. den Breejen, M. Versluijs-Helder, A.J. van Dillen, P.E. de Jongh, K.P. de Jong, Angew. Chem. Int. Ed. 46 (2007) 4547.
[9] L. Miersch, M. Schlesinger, R.W. Troff, C.A. Schalley, T. Ruffer, H.R. Lang, D. Zahn, M. Mehring, Chem. Eur. J. 17 (2011) 6985.
[10] Z.L. Cheng, K.W.M. Siu, R. Guevremont, S.S. Berman, Org. Mass Spectrom. 27 (1992) 1370.
[11] R. Frański, Eur. J. Mass Spectrom. 12 (2006) 199.
[12] D. Schröder, J. Roithová, Angew. Chem. Int. Ed. 45 (2006) 5705.
[13] D. Schröder, J. Roithová, H. Schwarz, Int. J. Mass Spectrom. 254 (2006) 197.
[14] D. Schröder, M.C. Holthausen, H. Schwarz, J. Phys. Chem. B 108 (2004) 14407.
[15] J. Roithová, D. Schröder, J. Am. Chem. Soc. 129 (2007) 15311.
[16] D. Schröder, K.P. de Jong, J. Roithová, Eur. J. Inorg. Chem. (2009) 2121.
[17] O. Dopfer, J. Phys. Org. Chem. 19 (2006) 540.
[18] L. MacAleese, P. Maitre, Mass Spectrom. Rev. 26 (2007) 583.
[19] N.C. Polfer, J. Oomens, Mass Spectrom. Rev. 28 (2009) 468.
[20] J. Oomens, L. Myers, R. Dain, C. Leavitt, V. Pham, G. Gresham, G. Groenewold, M. Van Stipdonk, Int. J. Mass Spectrom. 273 (2008) 24.
[21] G.S. Groenewold, J. Oomens, W.A. de Jong, G.L. Gresham, M.E. Mcllwain, M.J. Van Stipdonk, Phys. Chem. Chem. Phys. 10 (2008) 1192.
[22] C.M. Leavitt, J. Oomens, R.P. Dain, J. Steill, G.S. Groenewold, M.J. Van Stipdonk, J. Am. Soc. Mass Spectrom. 20 (2009) 772.
[23] L. Ducháčková, D. Schröder, J. Roithová, Inorg. Chem. 50 (2011) 3153.
[24] P. Milko, J. Roithová, D. Schröder, J. Lemaire, H. Schwarz, M.C. Holthausen, Chem. Eur. J. 14 (2008) 4318.
[25] P. Milko, J. Roithová, N.G. Tsierkezos, D. Schröder, J. Am. Chem. Soc. 130 (2008) 7186.
[26] E. Rezabal, L. Ducháčková, P. Milko, M.C. Holthausen, J. Roithová, Inorg. Chem. 49 (2010) 8421.
[27] A. Tintaru, J. Roithová, D. Schröder, L. Charles, I. Jušinski, Z. Glasovac, M. Eckert-Maksić, J. Phys. Chem. 112 (2008) 12097.
[28] N.B. Cech, C.G. Enke, Mass Spectrom. Rev. 20 (2001) 362.
[29] D. Schröder, T. Weiske, H. Schwarz, Int. J. Mass Spectrom. 219 (2002) 729.
[30] R.A.J. O'Hair, Chem. Commun. (2006) 1469.
[31] Á. Révész, P. Milko, J. Žabka, D. Schröder, J. Roithová, J. Mass Spectrom. 45 (2010) 1246.
[32] E.-L. Zins, C. Pepe, D. Schröder, J. Mass Spectrom. 45 (2010) 1253.
[33] L. Mac Aleese, A. Simon, T.B. McMahon, J.M. Ortega, D. Scuderi, J. Lemaire, P. Maitre, Int. J. Mass Spectrom. 249 (2006) 14.
[34] B. Chiavarino, M.E. Crestoni, S. Fornarini, F. Lanucara, J. Lemaire, P. Maitre, Angew. Chem. Int. Ed. 46 (2007) 1995.
[35] A. Simon, L. Aleese, P. Maitre, J. Lemaire, T.B. McMahon, J. Am. Chem. Soc. 129 (2006) 2829.
[36] J. Roithová, P. Milko, C.L. Ricketts, D. Schröder, T. Besson, V. Dekoj, M. Bělohradský, J. Am. Chem. Soc. 129 (2007) 10141.
[37] E.C. Tyo, A.W. Castleman, D. Schröder, P. Milko, J. Roithová, J.M. Ortega, M.A. Cinellu, F. Cocco, G. Minghetti, J. Am. Chem. Soc. 131 (2009) 13009.
[38] D. Schröder, H. Schwarz, P. Milko, J. Roithová, J. Phys. Chem. A 110 (2006) 8346.
[39] D. Schröder, L. Ducháčková, I. Jušinski, M. Eckert-Maksić, J. Heyda, L. Tůma, P. Jungwirth, Chem. Phys. Lett. 490 (2010) 14.
[40] L. Jiang, T. Wende, R. Bergmann, G. Meijer, K.R. Asmis, J. Am. Chem. Soc. 132 (2010) 7398.
[41] A.D. Becke, J. Chem. Phys. 98 (1993) 5648.
[42] S.H. Vosko, L. Wilk, M. Nusair, Can. J. Phys. 58 (1980) 1200.
[43] C. Lee, W. Yang, R.G. Parr, Phys. Rev. B 37 (1988) 785.
[44] B. Miehlich, A. Savin, H. Stoll, H. Preuss, Chem. Phys. Lett. 157 (1989) 200.
[45] Gaussian 03, Revision C.02, Gaussian, Inc., Wallingford, CT, 2004.
[46] J.P. Merrick, D. Moran, L. Radom, J. Phys. Chem. A 111 (2007) 11683.
[47] T.J. Lee, J.E. Rice, J. Phys. Chem. 96 (1992) 650.
[48] K.P. Jensen, Inorg. Chem. 47 (2008) 10357.
[49] N. Tsierkezos, D. Schröder, H. Schwarz, J. Phys. Chem. A 107 (2003) 9575.
[50] D. Schröder, H. Schwarz, Can. J. Chem. 83 (2005) 1936.
[51] B.M. Collins, AIP Conf. Proc. 430 (1998) 695.
[52] S.F. Levochkin, P.R. Smirnov, V.N. Trostin, Russ. J. Gen. Chem. 75 (2005) 1180.
[53] D. Schröder, O. Souvi, E. Alikhani, Chem. Phys. Lett. 470 (2009) 162.
[54] L. Ducháčková, J. Roithová, P. Milko, J. Žabka, N. Tsierkezos, D. Schröder, Inorg. Chem. 50 (2011) 771.
[55] D. Agrawal, E.-L. Zins, D. Schröder, Chem. Asian J. 5 (2010) 1667.
[56] P. Pietrzyk, M. Srebro, M. Radon, Z. Sojka, A. Michalak, J. Phys. Chem. A 115 (2011) 2316.
[57] B. Jagoda-Cwiklik, P. Jungwirth, L. Rulíšek, P. Milko, J. Roithová, J. Lemaire, P. Maitre, J.M. Ortega, D. Schröder, Chem. Phys. Chem. 8 (2007) 1629.

[58] N.G. Tsierkezos, J. Roithová, D. Schröder, M. Ončák, P. Slavíček, Inorg. Chem. 48 (2009) 6287.
[59] D. Smith, D. James, J. Devlin, J. Chem. Phys. 54 (1971) 4437.
[60] P. Milko, J. Roithová, J. Am. Chem. Soc. 132 (2010) 281.
[61] M. Ončák, D. Schröder, P. Slavíček, J. Comp. Chem. 31 (2010) 2294.
[62] D. Schröder, H. Schwarz, Angew. Chem. Int. Ed. Engl. 29 (1990) 1431.
[63] B. Butschke, M. Schlangen, H. Schwarz, D. Schröder, Z. Naturf. B 62b (2007) 309.
[64] C.L. Ricketts, D. Schröder, C. Alcaraz, J. Roithová, Chem. Eur. J. 14 (2008) 4779.
[65] Á. Révész, D. Schröder, J. Svec, M. Wimmerová, V. Šindelář, J. Phys. Chem. A 115 (2011) 11378.
[66] D. Schröder, L. Ducháčková, J. Tarábek, M. Karwowska, K. Fijalkowski, M. Ončák, P. Slavíček, J. Am. Chem. Soc. 133 (2011) 2444.
[67] J. Paterová, J. Heyda, P. Jungwirth, C.J. Shaffer, Á. Révész, E.L. Zins, D. Schröder, J. Phys. Chem. A 115 (2011) 6813.
[68] T.A. Rokob, L. Rulíšek, J. Šrogl, Á. Révész, E.L. Zins, D. Schröder, Inorg. Chem. 50 (2011) 9968.
[69] See also: R.K. Sinha, E. Nicol, V. Steinmetz, P. Maitre, J. Am. Soc. Mass Spectrom. 21 (2010) 758.